Journal of Solid State Chemistry 181 (2008) 2516–2522

Contents lists available at ScienceDirect

Journal of Solid State Chemistry

journal homepage: www.elsevier.com/locate/jssc

Hierarchical chlorine-doped rutile TiO_2 spherical clusters of nanorods: Large-scale synthesis and high photocatalytic activity

Hua Xu [a], Zhi Zheng [b], Lizhi Zhang [a,*], Hailu Zhang [c], Feng Deng [c]

[a] Key Laboratory of Pesticide and Chemical Biology of Ministry of Education, College of Chemistry, Central China Normal University, Wuhan 430079, PR China
[b] Institute of Surface Micro and Nano Materials, Xuchang University, Xuchang 461000, PR China
[c] State Key Laboratory of Magnetic Resonance and Atomic and Molecular Physics, Wuhan Institute of Physics and Mathematics, Chinese Academy of Sciences, Wuhan 430071, PR China

ARTICLE INFO

Article history:
Received 3 March 2008
Received in revised form
5 June 2008
Accepted 11 June 2008
Available online 13 June 2008

Keywords:
TiO_2
Hierarchical structures
Nanorods
Chlorine-doping
Photocatalysis

ABSTRACT

In this study, we report the synthesis of hierarchical chlorine-doped rutile TiO_2 spherical clusters of nanorods photocatalyst on a large scale via a soft interface approach. This catalyst showed much higher photocatalytic activity than the famous commercial titania (Degussa P25) under visible light ($\lambda > 420$ nm). The resulting sample was characterized by X-ray diffraction (XRD), scanning electron microscopy (SEM), transmission electron microscopy (TEM), high-resolution TEM (HRTEM), nitrogen adsorption, X-ray photoelectron spectroscopy (XPS), UV–vis diffuse reflectance spectroscopy, ^1H solid magic-angle spinning nuclear magnetic resonance (MAS-NMR) and photoluminescence spectroscopy. On the basis of characterization results, we found that the doping of chlorine resulted in red shift of absorption and higher surface acidity as well as crystal defects in the photocatalyst, which were the reasons for high photocatalytic activity of chlorine-doped TiO_2 under visible light ($\lambda > 420$ nm). These hierarchical chlorine-doped rutile TiO_2 spherical clusters of nanorods are very attractive in the fields of environmental pollutants removal and solar cell because of their easy separation and high activity.
© 2008 Elsevier Inc. All rights reserved.

1. Introduction

Photocatalytic technology has attracted worldwide research interest for the degradation of toxic pollutants in water, air and soil [1–3]. Among the various photocatalysts, TiO_2 has proven to be the benchmark photocatalyst because of its nontoxicity, chemical inertness, high efficiency, low cost and environmentally friendly features. It has widespread applications including water splitting, solar cell, mineralization of toxic organic substances, and so on [4,5]. However, the large band gap of titania photocatalyst makes it only active under ultraviolet irradiation ($\lambda < 388$ nm), accounting for a very small part ($< 5\%$) of the solar light energy. Therefore, the photocatalytic activity of TiO_2 need to be further improved for the practical applications [6]. In view of the efficient utilization of solar energy, it is still a challenge to develop TiO_2 photocatalysts highly active under solar light.

Nonmetal atoms-doped TiO_2 photocatalysts have attracted more and more attention since Asahi and coworkers reported the N-doped TiO_2 visible light photocatalyst in 2001 [7]. For example, C [8], N [9], S [10], F [11], I [12] and Br/Cl [13]-doped TiO_2 photocatalysts have been reported in recent years. Some of these nonmetal dopings can extend the absorption of TiO_2 to visible light region and make TiO_2 active under visible light irradiation. On the other hand, some researches found that the oxygen vacancies or other surface defects originated from the nonmetal dopants may account for visible light photocatalytic activity of the doped photocatalyst, other than their absorption extensions to visible light region. For instance, Yu and coworkers observed an effective degradation of 4-chlorophonel over hierarchical nanoporous F-doped TiO_2 under visible light illumination. They attributed this visible light photocatalytic activity to extrinsic absorption through the creation of oxygen vacancies because F-doping did not produce any effect on the optical absorption extension to visible light in that study [14]. In the previous report, Chen et al. calcined the gel formed by the hydrolysis of tetrabutyl titanate in hydrochloric acid at different temperatures to obtain a chlorine-doped TiO_2 catalyst, the product was either a mixture of anatase–amphous or a mixture of anatase–rutile [15].

Recently, we found the soft interface of water and chloroform could be utilized as a general platform to prepare hierarchical inorganic spherical nanostructures [16]. In this study, this soft interface method was developed to synthesize hierarchical chlorine-doped rutile TiO_2 spherical clusters of nanorods on a large scale. The activity of the resulting sample was about four times of the famous high active commercial photocatalyst Degussa P25 under visible light irradiation. This hierarchical

* Corresponding author. Fax: +86 27 6786 7535.
E-mail address: zhanglz@mail.ccnu.edu.cn (L. Zhang).

0022-4596/$ - see front matter © 2008 Elsevier Inc. All rights reserved.
doi:10.1016/j.jssc.2008.06.019

chlorine-doped rutile TiO_2 spherical clusters of nanorods photocatalyst is an exciting new member in the family of nonmetal-doped TiO_2 photocatalysts. To the best of our knowledge, this is the first report on the synthesis of chlorine-doped rutile TiO_2 spherical clusters of nanorods with high photocatalytic activity on a large scale.

2. Experimental section

2.1. Sample preparation

All chemicals were of analytical grade and used as received. P25 TiO_2 (a mixture of 70% anatase and 30% rutile, surface area: about $50 \pm 5\ m^2/g$) was purchased from Degussa (Germany).

Hierarchical chlorine-doped rutile TiO_2 spherical clusters of nanorods (denoted as Cl-TiO_2) were synthesized by a hydrothermal method by using $TiCl_4$ as the starting material. Typically, 5 mL of $TiCl_4$ was slowly added into 25 mL of deionized water at 4 °C to prepare a $TiCl_4$ aqueous solution. The resulting solution was added to 50 mL of chloroform in 100-mL Teflon-line stainless autoclave. The autoclave was conducted in the temperature 150 °C for 12 h, and then air-cooled to room temperature. The product formed between the layers of water and chloroform was collected by centrifugation and washed with deionized water and ethanol, and finally dried at 50 °C in air for 12 h to obtain white powder. The yield of Cl-TiO_2 powder was more than 98%. Ten grams of Cl-TiO_2 could be easily produced in our laboratory.

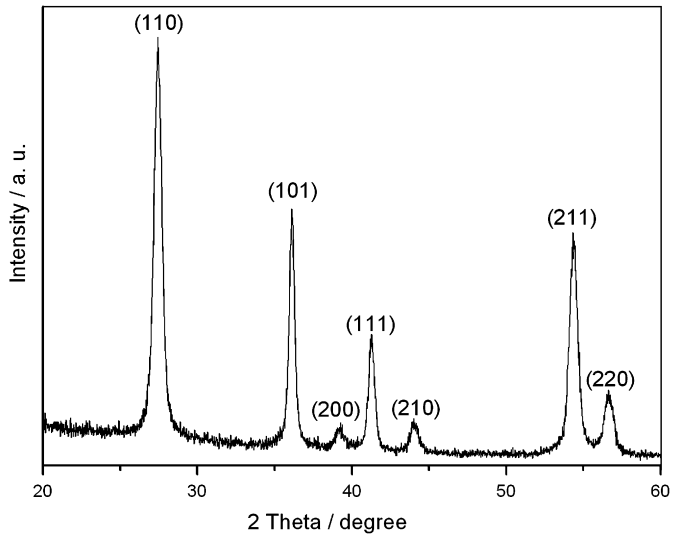

Fig. 1. Powder XRD pattern of the as-prepared sample.

2.2. Characterization

The powder X-ray diffraction (XRD) pattern was recorded on a Rigaku D/MAX-RB diffractometer with monochromatized Cu$K\alpha$ radiation ($\lambda = 1.5418$ Å). Scanning electron microscopy (SEM, JSM-5600) was used to characterize the morphology of the samples. Transmission electron microscopy (TEM) study was carried out on a Philips CM-120 electron microscopy instrument. The samples for TEM were prepared by dispersing the final powders in ethanol; the dispersion was then dropped on carbon–copper grids. High-resolution transmission electron microscopy (HRTEM) measurement was performed using a high-resolution transmission electron microscope (HRTEM; JEOL JSM-2010 microscope) operated at an acceleration voltage of 200 kV. The nitrogen adsorption and desorption isotherms at 77 K were measured using a Micrometritics ASAP2010 system after samples were vacuum-dried at 473 K overnight. X-ray photoelectron spectroscopy (XPS) measurements were performed in a VG Scientific ESCALAB Mark II spectrometer equipped with two ultra-high vacuum chambers. All the binding energies were calibrated to the C1s peak at 284.8 eV of the surface adventitious carbon. A Varian Cary 100 Scan UV–visible system equipped with a labsphere diffuse reflectance accessory was used to obtain the reflectance spectra of the catalysts over a range of 200–800 nm. Lab sphere USRS-99-010 was employed as a reflectance standard. The spectra were converted from reflection to absorbance by Kubelka–Munk method. ^1H solid magic-angle spinning nuclear magnetic resonance (MAS NMR) measurements were performed with a 5 mm probe on a Varian Infinityplus-400 spectrometer. ^1H MAS NMR

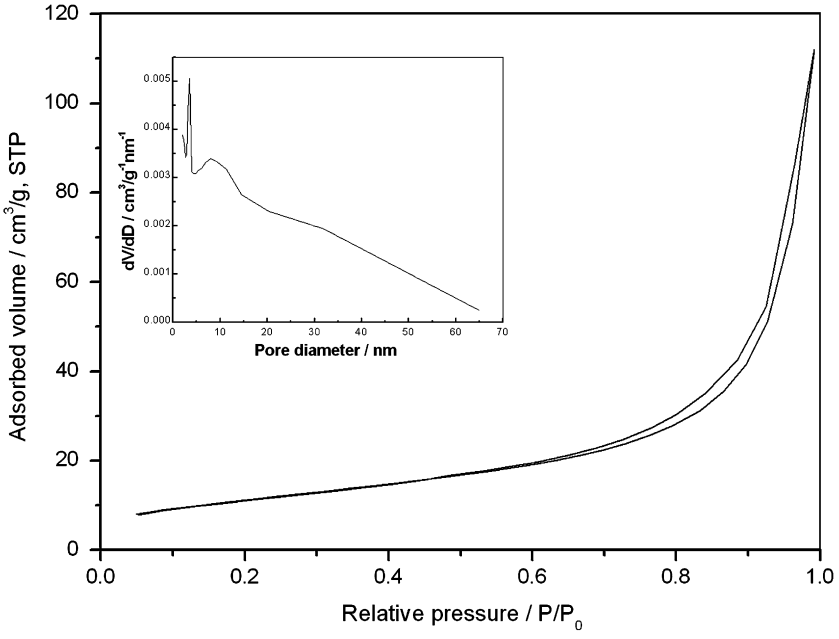

Fig. 2. Nitrogen adsorption–desorption isotherms and the corresponding pore size distribution curve (inset) of Cl-TiO_2.

spectra were acquired using one pulse with a ^{1}H pulse width ($\pi/2$) of 4.3 μs, a 5 s pulse delay was given, and 1000 scans. A sample was first placed in glass tubes connected to a vacuum. The temperature was slowly (1.5 K/min) increased to 673 K and held in a vacuum for 4 h to dehydrate the material. After the sample cooled to room temperature, glass tube was sealed. And then the sealed sample was transferred into a ZrO_2 NMR rotor under a dry nitrogen atmosphere in a glove box. Proton chemical shifts were referenced to TMS as an external standard. The photoluminescence (PL) emission spectra were measured at room temperature with a 10-Mw and 325-nm He–Cd laser.

2.3. Photocatalytic activity test

The photocatalytic activities of the samples were evaluated by the degradation of rhodamine B (RhB) in an aqueous solution. A 500-W tungsten halogen lamp was positioned inside a cylindrical vessel and surrounded by a circulating water jacket to cool it. A 0.1 g amount of photocatalyst was suspended in a 100 mL aqueous solution of 5 mg/L RhB. The solution was continuously stirred for about 1 h to ensure the establishment of an adsorption–desorption equilibrium among the photocatalyst, RhB and water before irradiation, then the solution was shined with

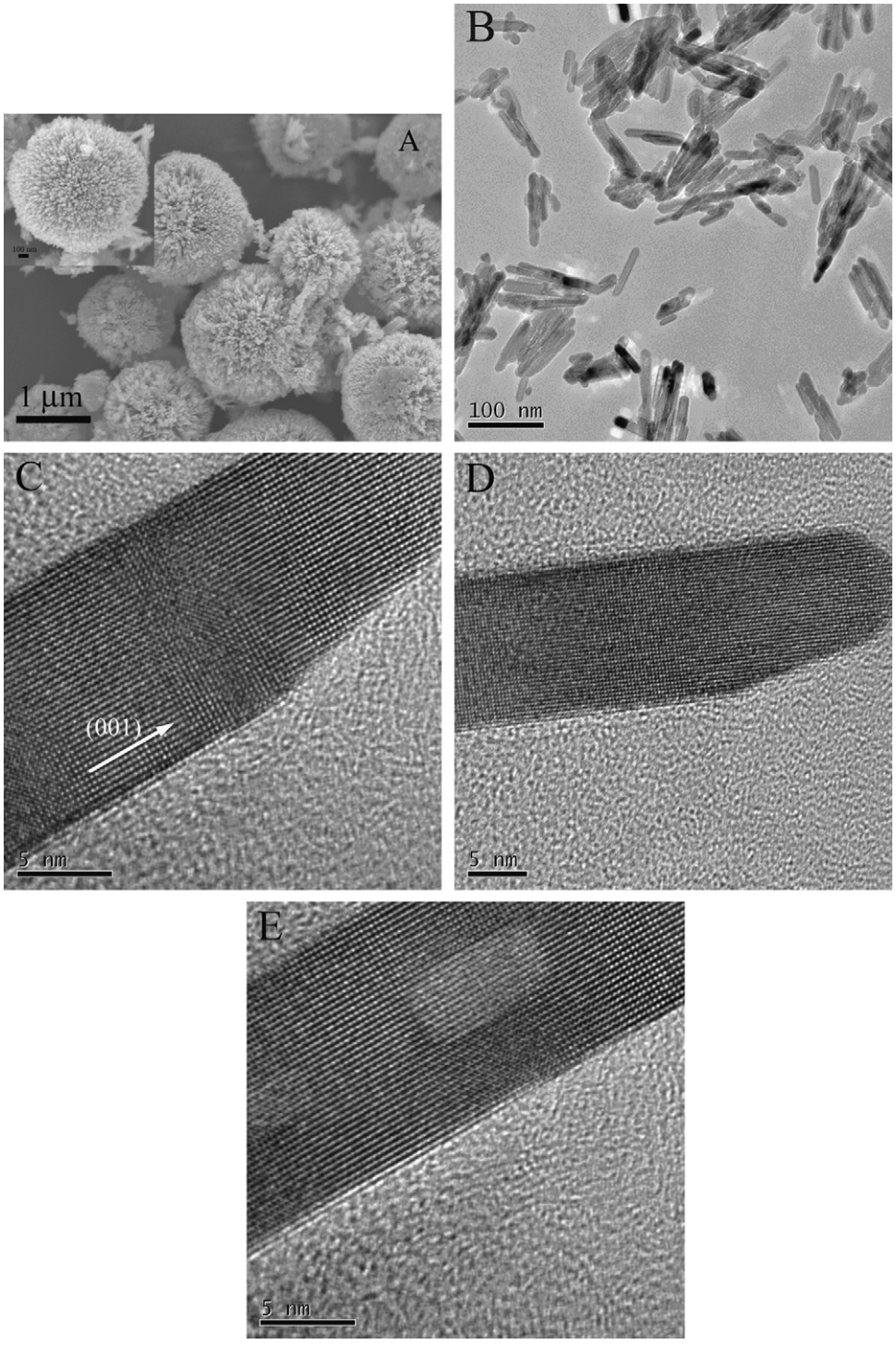

Fig. 3. SEM (A), TEM (B) and HRTEM (C–E) images of Cl-TiO_2.

visible light from the tungsten halogen lamp with a 420-nm-cutoff filter to remove UV radiation from the lamp. The distance between light source and the bottom of the solution was about 15 cm, and the temperature of the RhB solution stirred by a dynamoelectric stirrer in an open reactor was about 25 °C. The concentration of RhB was monitored by colorimetry with a U-3310 UV–vis spectrometer (HITACHI).

3. Results and discussion

The XRD was used to identify the phase structure of the as-prepared sample (Cl-TiO_2). Fig. 1 shows the XRD pattern of the as-prepared sample. All the peaks of XRD pattern can be readily indexed to rutile TiO_2 (JCPDS file no. 86-0147). The peaks at 27.43°, 36.08°, 39.19°, 41.24°, 44.04°, 54.32°, 56.62° are assigned to (110), (101), (200), (111), (210), (211), (220) planes of rutile TiO_2, respectively. The average crystal sizes of Cl-TiO_2 are about 28 nm determined from the broadening of the (110) peak by the Scherrer formula.

Fig. 2 presents the nitrogen adsorption–desorption isotherms and Barret–Joyner–Halenda pore size distribution curve (inset) of Cl-TiO_2. The adsorption isotherms can be classified as type III with hysteresis loops, which may be caused by the weak adsorbate–adsorbate interactions [17]. There is a hysteresis loop in the isotherm, corresponding to the filling of pores produced by the agglomeration of the particles. The Brunauer–Emmett–Teller specific surface area of Cl-TiO_2 is 41 m^2/g. This value is comparable to that (about 50 ± 5 m^2/g) of P25.

SEM was used to characterize the morphology of the sample. Spherical particles of micrometer size were observed in the Cl-TiO_2 sample (Fig. 3A). The spheres are composed of agglomerated nanorods of 20–30 nm in diameters (inset of Fig. 3A), confirming the result of nitrogen adsorption. The yield of nanorods in the sample was as high as about 100% according to the SEM observation. Fig. 3B shows a typical TEM image of Cl-TiO_2, which reveals that the Cl-TiO_2 rods are 10–30 nm in diameters and 100–150 nm in lengths. The growth direction of the nanorods is found to be along (001) direction with (110) plane exposing outside according to HRTEM image (Fig. 3C). This is reasonable because (110) plane of rutile TiO_2 is known to be the thermodynamically most stable, that is, to have the lowest surface Gibbs energy. Interestingly, line defects or dislocations including screw dislocations (Fig. 3C) and edge dislocations (Fig. 3D) were found on the HRTEM images. Besides dislocations, the stacking faults could also be observed (Fig. 3E). These crystal defects were probably resulted from high strain energy caused by the Cl doping. It is known that many factors such as the differences between atomic radius and electronegativity can induce lattice distortions which further lead to high strain energy. Because significant difference exists between the atomic radii of the dopant Cl (1.81 Å) and O (1.32 Å), the cell parameters would change with the increase on the concentration of the dopant. When there are certain gradients along the concentration distribution of the dopant Cl in rutile TiO_2, the two neighboring lists of oxygen ions perpendicular to the concentration gradients of Cl cannot match well any more. This would result in large lattice distortions, arising high strain energy in TiO_2. As soon as the strain energy exceeds the elastic deformation limit of crystals, dislocations and stack faults would arise to overcome the strain energy caused by lattice distortions.

Fig. 4A shows the XPS survey spectrum of the Cl-TiO_2. The peaks related to Ti, O, carbon elements and a trace amount of Cl could be observed. Fig. 4B gives the high-resolution XPS spectrum of Cl 2p. The peak around 198 eV is corresponding to the Cl $2p_3$, which reveals the existence of Cl^-. The atomic ratio of Cl to Ti was calculated to be about 2:98 on the basis of XPS analysis.

Fig. 5 shows the plots of the $(ahv)^{1/2}$ versus the energy of absorbed light and diffuse reflectance absorption spectra (inset) of Cl-TiO_2 and P25. Assuming the Cl-TiO_2 to be indirect semiconductors, like TiO_2, the plots of the $(ahv)^{1/2}$ versus the energy of absorbed light affords band-gap energies of the samples. The band gaps optically obtained in such a way were approximately of 2.99 and 3.17 eV for Cl-TiO_2 and P25, respectively. Therefore, Cl-TiO_2 possesses a slight red-shift absorption edge than P25.

The surface acidity of a photocatalyst could greatly effect its photocatalytic activity [18–20]. It is known that ^1H MAS NMR can detect the surface acidity of solid samples. So we measured the ^1H MAS NMR spectra of Cl-TiO_2 and P25 (Fig. 6). In ^1H MAS NMR spectra of various samples, signals from different surface OH groups bound to certain elements are often resolved, thus allow an accurate measurement of their chemical shifts. The metal oxide suspensions are known to be amphoteric, so they could be considered diprotic acids [21]. For TiO_2, the principal amphoteric surface functionality is the "titanol" moiety TiOH. Hydroxyl groups on the TiO_2 surface undergo the following acid–base equilibria (1):

$$TiOH_2^+ \leftrightarrow TiOH + H^+ \quad (1)$$

$$TiOH \leftrightarrow TiO^- + H^+ \quad (2)$$

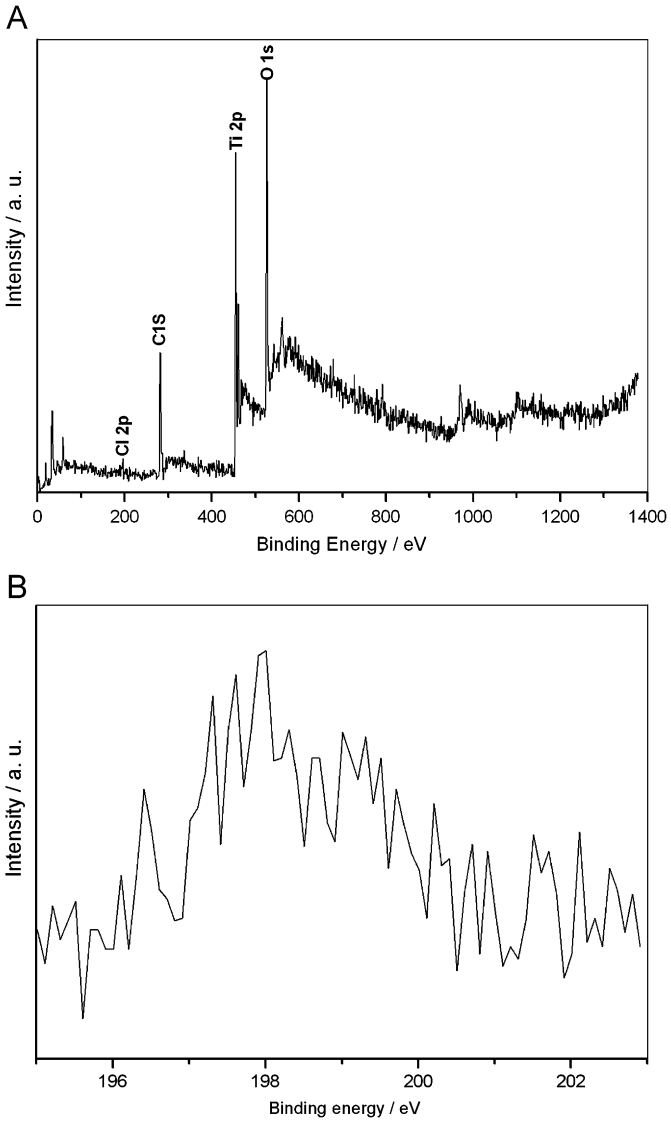

Fig. 4. XPS spectra of the Cl-TiO_2 sample: (A) survey and (B) high-resolution spectra of Cl 2p.

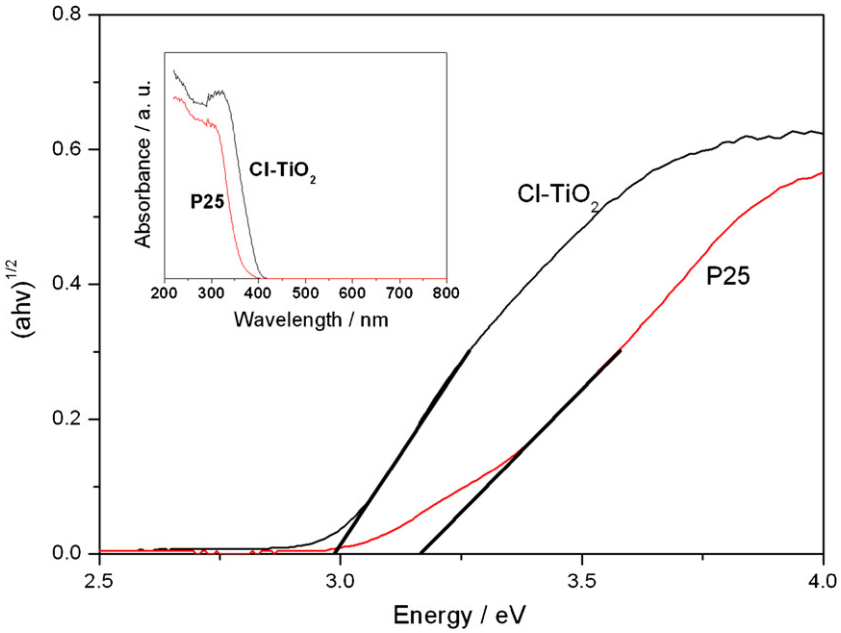

Fig. 5. Plots of the $(ahv)^{1/2}$ versus the energy of absorbed light and diffuse reflectance absorption spectra (inset) of Cl-TiO_2 and P25.

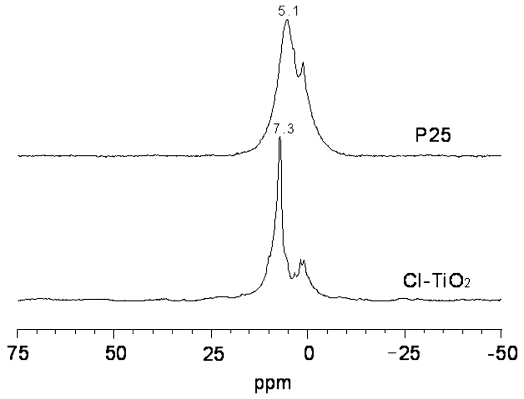

Fig. 6. ^{1}H MAS NMR spectra of Cl-TiO_2 and P25.

There are two types OH groups on the TiO_2 surface. For Cl-TiO_2, the downfield peak located at 7.3 ppm can be attributed to acidic OH groups coordinated to two Ti atoms, while the signals at 1.8 and 1.1 ppm more likely belong to basic OH groups coordinated one Ti atom [22]. The low field peak most probably can be ascribed to the more acidic OH groups [23]. We can see from Fig. 6 that Cl-TiO_2 (7.3 ppm) has a lower field peak than P25 (5.4 ppm), which indicates that as-prepared Cl-TiO_2 demonstrated a stronger acidity than P25.

Photodegradation of RhB was used as a model reaction to compare the photocatalytic activities of Cl-TiO_2 and P25. Fig. 7 shows the decrease of the concentration of RhB with irradiation time in the presence of Cl-TiO_2 and P25 as well as self-degradation of RhB in the absence of any photocatalyst under visible light ($\lambda > 420$ nm) irradiation. It was found that the self-degradation of RhB was negligible under visible light ($\lambda > 420$ nm). However, 85% and 20% of RhB were degraded in the presence of Cl-TiO_2 and P25 after 4 h of reaction time under visible light ($\lambda > 420$ nm) irradiation, respectively. Therefore, Cl-TiO_2 showed much higher photocatalytic activity. Its activity was about four times of that of P25. Moreover, during the photodegradation experiments the micrometer-sized hierarchical structures of Cl-TiO_2 make its separation from the water much easier than that of P25 with sizes in nanometer scale. This characteristic is very important for

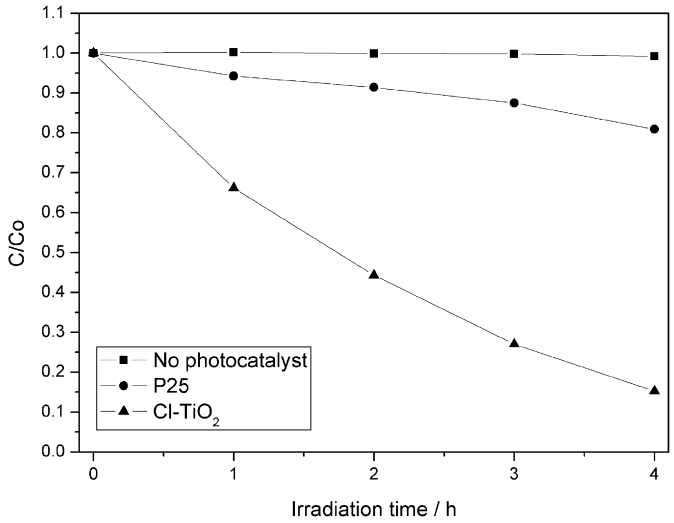

Fig. 7. Photodegradation of RhB in the presence of the Cl-TiO_2 and P25 photocatalysts as well as self-degradation of RhB in the absence of any photocatalyst under visible light irradiation ($\lambda > 420$ nm).

the practical application of photocatalysts in the field of wastewater treatment.

In our previous study, we proposed a possible process to explain the formation of hierarchical rutile TiO_2 nanoarchitectures [16]. This possible formation process may include four steps: (1) formation of TiO_2 nanoparticles; (2) formation and stabilization of chloroform/water emulsion; (3) growth of rutile TiO_2 nanorods and (4) their self-assembly into hierarchical spheres. At the beginning of the reaction, TiO_2 nanoparticles formed by the forced hydrolysis of $TiCl_4$ at elevated temperature. Meanwhile, spherical emulsions may form at the interface region of bulk water/chloroform because of the extreme condition during hydrothermal treatment. The preformed TiO_2 nanoparticles would enter the emulsions and/or stay at interfacial surfaces of the emulsions. Like the surfactants, these TiO_2 nanoparticles at the interfacial region of the emulsions could stabilize these emulsions and subsequently serves as the sites for the growth of TiO_2 nanorods in the

emulsions or on the interface of the emulsions. Because the interface of the emulsion could enrich the components from bulk solutions, TiO_2 nanorods growth on the interface of the emulsions should be faster than that in the emulsions. With the growth of nanorods, the nanorods also self-assembled into hierarchical architectures with aligned orientation in order to minimize surface energy. Because of the confinement effect of the emulsions, most of the final hierarchical architectures possess spherical shape [16].

In our synthesis, $CHCl_3$ was used to create the soft interface. During the synthesis, some $CHCl_3$ molecules would be decomposed into HCOH, HCl and other mineralized products under hydrothermal treatment [24]. Meanwhile, the hydrolysis of $TiCl_4$ also produced a large amount of Cl^-. Therefore, the abundant Cl^- in the reaction media would be adsorbed on the surface of the fresh TiO_2 primary nanoparticles formed by the forced hydrolysis of $TiCl_4$. During the subsequent growth of TiO_2 nanorods from these primary nanoparticles and assembly of TiO_2 nanorods into hierarchical spheres, some Cl^- adsorbed on the surface of TiO_2 primary nanoparticles would substitute the O in the lattices of TiO_2 nanorods or embedded into the matrix. Although we could not calculate the accurate ratios of Cl^- with different environments (in the lattices or embedded into the matrix) in hierarchical TiO_2 spherical clusters of nanorods because of its low content, XPS already confirmed the existence of Cl^- in the resulting sample (Fig. 4B). These substituted Cl would cause the lattice distortion because of their larger atomic radii than those of O, thus resulted in some defects in the TiO_2, which was confirmed by the HRTEM measurements (Fig. 3).

It is known that the photocatalytic activity of titania is affected by many factors such as surface area, phase structure, crystallinity, surface hydroxyl density, surface acidity, surface defects, and so on. On the basis of the above characterizations, we attributed the high photocatalytic activity of Cl-TiO_2 to several reasons as follows. First, the extended absorption edge of Cl-TiO_2 made it absorb more visible light and easily be excited. Once excited, the electrons and holes are generated on the surface of the photocatalysts which is favorable for the photoreaction. Second, Cl-TiO_2 possessed higher surface acidity than P25, as revealed by ^1H MAS NMR spectra (Fig. 6). It was claimed that a catalyst with an acidic surface can easily adsorb polar organic molecules for photoactivity enhancement [19,20]. Meanwhile, more adsorbed organic molecules may inhibit the recombination of photogenerated electron–hole pairs. Finally, it is known that the existence of crystal defects is regarded as one of the important reasons associated with the high activity [25]. In our case, because the defects of rutile TiO_2 nanorods were created by replacing O^{2-} with Cl^-, these defects might also promote the better separation of photogenerated electron–hole pairs by trapping the electrons. This better separation was confirmed by PL emission spectra of Cl-TiO_2 and P25 (Fig. 8). It was found that Cl-TiO_2 exhibited much lower emission intensity than P25, suggesting the recombination rate of photogenerated electron–hole pairs was slower in Cl-TiO_2 than in P25 [11]. It was also reported that the formation of $^{\bullet}OH$ was favored on nonmetal-doped TiO_2 because more active sites could be created. Moreover, the nonmetal-dopant atoms increased the photogenerated electron mobility [26], which was consistent with our result in this study.

4. Conclusions

In this study, we successfully produced highly active chlorine-doped rutile TiO_2 spherical clusters of nanorods photocatalyst via a soft interface method. The soft interface was created with two immiscible phases of $CHCl_3$ and H_2O. This interesting soft interface not only produced hierarchical spherical clusters of nanorods, but also resulted in Cl doping in TiO_2. The Cl doping further extended the absorption edge of TiO_2 and caused higher surface acidity and crystal defects in TiO_2, which were the major reasons for the high photocatalytic activity of hierarchical chlorine-doped TiO_2 spherical clusters of nanorods photocatalyst. This study provides a low temperature method to prepare highly active photocatalysts on a large scale. The hierarchical chlorine-doped TiO_2 spherical clusters of nanorods are very promising for environmental pollutants removal and solar cell [27] because of their easy separation and high activity.

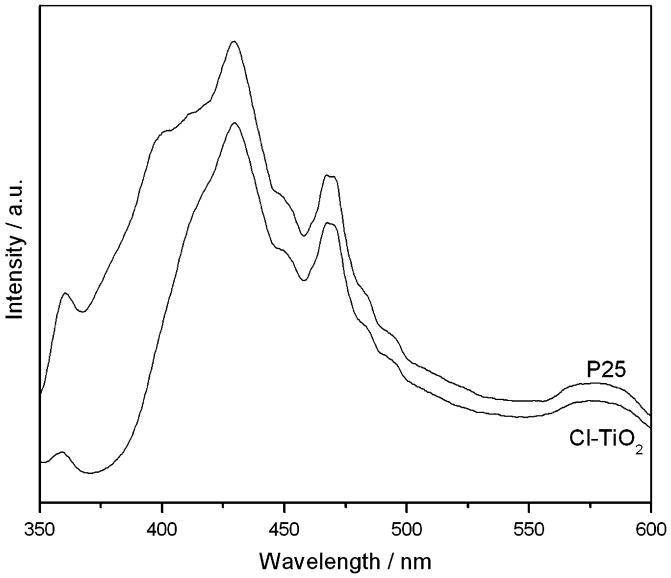

Fig. 8. PL emission spectra of Cl-TiO_2 and P25.

Acknowledgments

This work was supported by National Basic Research Program of China (973 Program) (Grant 2007CB613301), National Science Foundation of China (Grants 20503009 and 20777026), Program for New Century Excellent Talents in University (Grant NCET-07-0352), and the Key Project of Ministry of Education of China (Grant 108097). We thank Dr. Z. S. Li (Ecomaterials and Renewable Energy Research Center, Department of Physics, Nanjing University) for his kind help on HRTEM analysis.

References

[1] M.R. Hoffmann, S.T. Martin, W.Y. Choi, D.W. Bahnemann, Chem. Rev. 95 (1995) 69.
[2] A.L. Linsebigler, G.Q. Lu, J.T. Yates, Chem. Rev. 95 (1995) 735.
[3] O.M. Alfano, D. Bahnemann, A.E. Cassano, R. Dillert, R. Goslich, Catal. Today 58 (2000) 199.
[4] A. Mills, S. LeHunte, J. Photochem. Photobiol. A: Chem. 108 (1997) 1.
[5] A. Fujishima, T.N. Rao, D.A. Tryk, J. Photochem. Photobiol. C: Photochem. Rev. 1 (2000) 1.
[6] H. Kominami, S. Murakami, J. Kato, Y. Kera, B. Ohtani, J. Phys. Chem. B 106 (2002) 10501.
[7] R. Asahi, T. Morikawa, T. Ohwaki, K. Aoki, Y. Taga, Science 293 (2001) 269.
[8] W.J. Ren, Z.H. Ai, F.L. Jia, L.Z. Zhang, X.X. Fan, Z.G. Zou, Appl. Catal. B: Environ. 69 (2007) 138.
[9] H. Irie, S. Washizuka, N. Yoshino, K. Hashimoto, Chem. Commun. (2003) 1298.
[10] J.C. Yu, W.K. Ho, J.G. Yu, H. Yip, P.K. Wong, J.C. Zhao, Environ. Sci. Technol. 39 (2005) 1175.
[11] J.C. Yu, J.G. Yu, W.K. Ho, Z.T. Jiang, L.Z. Zhang, Chem. Mater. 14 (2002) 3808.
[12] X.T. Hong, Z.P. Wang, W.M. Cai, F. Lu, J. Zhang, Y.Z. Yang, N. Ma, Y.J. Liu, Chem. Mater. 17 (2005) 1548.
[13] H.M. Luo, T. Takata, Y.G. Lee, J.F. Zhao, K. Domen, Y.S. Yan, Chem. Mater. 16 (2004) 846.

[14] W.K. Ho, J.G. Yu, S.C. Lee, Chem. Commun. (2006) 1115.
[15] H. Chen, M.C. Long, J. Xu, W.M. Cai, Chin. J. Catal. 27 (2006) 890.
[16] H. Xu, F.L. Jia, Z.H. Ai, L.Z. Zhang, Cryst. Growth Des. 7 (2007) 1216.
[17] K.S.W. Sing, D.H. Everett, R.A.W. Haul, L. Moscou, R.A. Pierotti, J. Rouquerol, T. Siemieniewska, Pure Appl. Chem. 57 (1985) 603.
[18] G. Martra, Appl. Catal. A: Gen. 200 (2000) 275.
[19] Y.T. Kwon, K.Y. Song, W.I. Lee, G.J. Choi, Y.R. Do, J. Catal. 191 (2000) 192.
[20] V. Keller, P. Bernhardt, F. Garin, J. Catal. 215 (2003) 129.
[21] C. Kormann, D.W. Bahnemann, M.R. Hoffmann, J. Phys. Chem. 92 (1988) 5196.
[22] K. Tanaka, J.M. White, J. Phys. Chem. 86 (1982) 4708.
[23] X.Z. Fu, L.A. Clark, Q. Yang, M.A. Anderson, Environ. Sci. Technol. 30 (1996) 647.
[24] J.C.S. Wong, A. Linsebigler, G.Q. Lu, J.F. Fan, J.T. Yates, J. Phys. Chem. 99 (1995) 335.
[25] D.M. Liu, Y.F. Zhu, L.Q. Li, Int. J. Hydrogen Energy 32 (2007) 2455.
[26] D. Li, H. Haneda, S. Hishita, N. Ohashi, N.K. Labhsetwar, J. Fluorine Chem. 126 (2005) 69.
[27] H.M. Jia, H. Xu, Y. Hu, Y.W. Tang, L.Z. Zhang, Electrochem. Commun. 9 (2007) 354.